Escola de Primavera de Transição e Turbulência
Blumenau 2020

ABCM Associação Brasileira de Engenharia e Ciências Mecânicas

12th Spring School on Transition and Turbulence
September 21st-25th, 2020, Blumenau, SC, Brazil

EPTT-2020-0018
NUMERICAL ANALYSIS OF IN-LINE TUBE BANK ASYMMETRIC FLOW

Roberta Fátima Neumeister
Adriane Prisco Petry
Sergio Viçosa Möller
Federal University of Rio Grande do Sul - PROMEC
roberta.neumeister@ufrgs.br
adrianep@mecanica.ufrgs.br
svmoller@ufrgs.br

Abstract. *The purpose of these study is to present a numerical analysis that shows three-dimensional asymmetric flow characteristics in a fixed in-line tube bank. The study was conducted using Large Eddy Simulation with sub grid scale model Smagorinski-Lilly and Dynamic stress with Ansys Fluent 19. The tube bank presents quadrangular configuration with spacing ratio 1.26. Reynolds number is 5 x 10^4, based on gap flow velocity and one-cylinder diameter. Results show asymmetry on the flow along the tube bank height, mainly after the second row of cylinders. Asymmetry is observed between the lines of cylinders, with flow redistribution, increasing and decreasing velocity inside the tube bank. This velocity and pressure distribution influence force distribution along the cylinders that may be the responsible for instability on cylinders free to vibrate.*

Keywords: *Numerical Analysis, Asymmetric flow, Tube bank.*

1. INTRODUCTION

Tube banks are common engineering structures and study of fixed arrays and free to vibrate arrays are necessary to understand the mechanisms of excitation, vibration and forces on the tubes (Blevins,1990 and Paidöussis, 2011). A study that presented asymmetry on the flow over tube banks was presented by Olinto et al. (2009) that reported an experimental study of the flow instabilities in the first rows of fixed tube banks. The pitch to diameter ratios p/d = 1.26 were studied with Reynolds number ranged between $3 \times 10^4 - 8 \times 10^4$. The main results showed the presence of instabilities, generated after the second row of the tube bank, which propagates to the interior of the bank. The resulting flow show that the three orthogonal components are equally significant. The Authors described that the three-dimensional behavior of the flow is responsible for a mass redistribution inside the bank that leads to velocity values not expected for the studied geometry.

Endres and Möller (2009) showed the propagation of a far-field perturbation in a tube bank adding vortex generators with a well-defined frequency. The authors observed that, by reducing the gap spacing, the disturbance was dissipated after the second row for the largest vortex generator. For the cases with the smallest vortex generator, with both vortex generators with the largest p/d-ratio studied, it subsisted until the 4^{th} or 5^{th} rows.

Iacovides et al. (2014) reported experiences from applying alternative strategies for modelling turbulent flow and local heat-transfer coefficients around in-line tube banks. The main objective was the flow simulation using large-scale tube banks with confining walls. It was found that the path taken by the fluid through the tube-bank configuration differs according to the treatment of turbulence and whether the flow is treated as two- or three-dimensional. The authors do not associate the change in the path with the random instabilities of the tube bank flow, but it could be related to the instabilities presented by Olinto et al. (2009).

Abed and Afgan (2017) presented the effect of changing the aspect ratio on the heat transfer and flow quantities over in-line tube banks. The authors showed that for the square pitch ratios, the solution has faced a gradual change from a strong asymmetric to asymmetric, then to a perfect symmetry. The strong asymmetric solution was found by the very narrow aspect ratio of 1.2. However, the behavior of cases with p/d = 1.5 and 1.6 became less strong than that predicted for the case of 1.2. For the larger aspect ratio of 1.75, the flow behavior is seen to be symmetric for all variables under consideration except Nusselt number. The asymmetry is associated by the authors to the blockage influences coming from the downstream tubes which act to highly destroy the vortex shedding, mainly for intermediate p/d. The locations of the separation shear layer different from each other which in turn led to provide an alternating asymmetrical behavior as presented in the flow patterns.

da Silva et al. (2019) presented a numerical study of the three-dimensional flow around an in-line cylinder arrangement with up to twenty-five cylinders under confinement, with a subcritical Reynolds number, in the context of flow-induced vibrations. Flow characteristics and patterns, as well as the force coefficients of the cylinders and Strouhal numbers were

evaluated numerically with the large eddy simulation. The authors describe a classification of main characteristics is ranges of rectangular p/d.

Blevins (1990) present the amplitude increase for tube arrays on airflow; describes that the onset of instability generally occurs well above the vortex resonance. Critical velocity increases up to 60% have been obtained by detuning adjacent tubes, but in other cases no increase occurs, and a single flexible cylinder surrounded by rigid tubes may or may not became unstable depending on characteristics of the array. Austermann and Popp (1994) reported the experimental investigations of fluid elastic instability in tube arrays subjected to air crossflow. The vibration behavior of one flexibly mounted tube within otherwise fixed bundles for the configurations normal and rotated triangular, in-line and rotated square. Results presented the stability boundaries of the flexibly mounted cylinder positioned in each of the first three or four rows of the different arrays, showing no vibration increase for in-line configuration with p/d=1.25. Paidöussis et al. (2011) presented a review on the available models to predict instabilities in tube arrays showing the positive and negative points in the models. In general, the Authors describe that there is room for improvement and number of issues to be addressed in each model.

Even with the number of models to predict the critical flow, there is not a clear description why the increase happens. A hypothesis is that the behavior of the flow in the gap and along the height of the tube bank influences the instability due the asymmetry of pressure field and forces. This mechanism would explain why with no change in the incoming flow velocity a free to vibrate tube inside the tube bank increases the amplitude of vibration. The study of the asymmetric flow in the tube bank can show the characteristics of these instabilities. Considering the expose, the purpose of these study is to present a numerical analysis of the three-dimensional crossflow over a fixed tube bank with a square space ratio 1.26 to study the asymmetric flow and the relation with force distribution inside the tube bank.

2. METHODOLOGY

The numerical analysis is executed using a domain with cross section of 0.146 x 0.193m and length of 0.8m, the domain presents twenty-five smooth cylinders and 10 half cylinders to close the section. The space ratio longitudinal and transversal is 1.26, the Reynolds number is 5 x 10^4, based on the gap flow velocity and one-cylinder diameter. These characteristics are presented in Figure 1a).

The mesh is generated using tetrahedral volumes including a region with additional refinement, prismatic layers in the cylinder and side walls, as presented in Figure 1 b), the mesh presents 21 million volumes. The y+ remain between 0.5 and 1.7 on the tubes. The boundary conditions are prescribed velocity inlet of 5m/s, atmospheric pressure in the outlet and wall with no slip condition for all the additional domain parts.

The simulations were executed using ANSYS Fluent 19 applying Large Eddy Simulation to solve mass conservation and momentum with sub grid scale model Smagorinski-Lilly with Dynamic stress (Wilcox, 1993, Lesieur et al. 2005 and ANSYS Fluent, 2018). The transient analysis is executed with time step 1 x10^{-5} s and the convergence criteria 10^{-6} for all monitored variables.

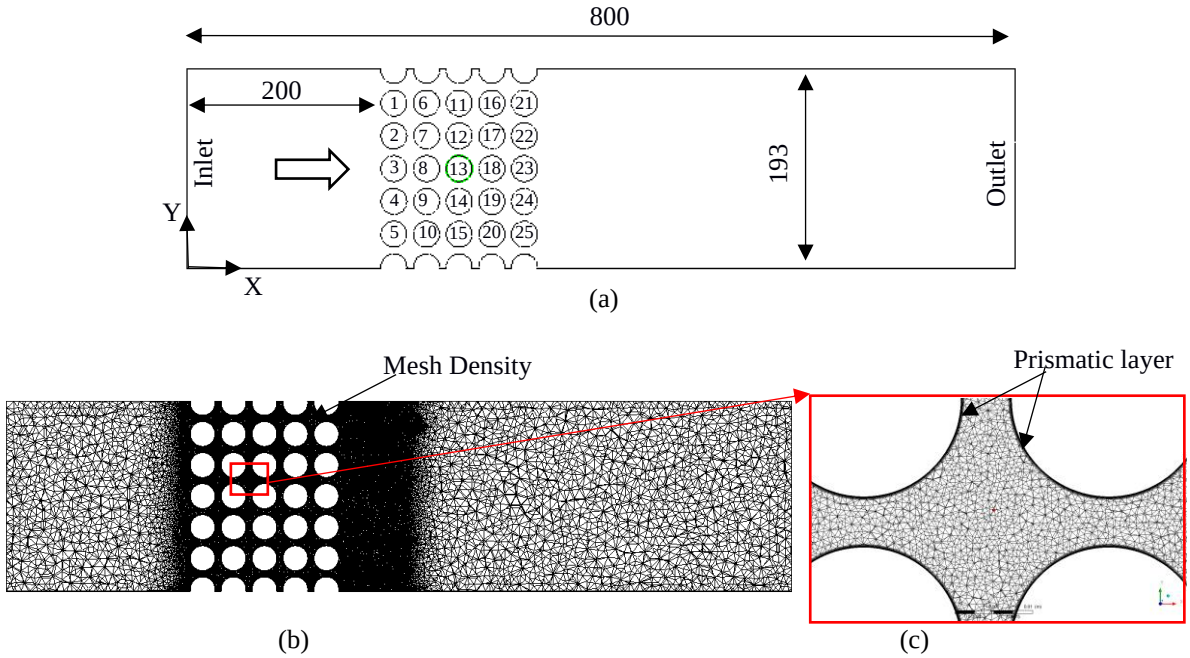

Figure 1. a) Domain size in milimeters and boundary conditions, b) Mesh with density region and c) Mesh detail with prismatic layer.

The velocity in the domain is monitored on the lines positioned inside the gaps between the cylinders, as observed in Figure 2 a), six lines are applied. The pressure and velocity are analyzed on planes along the height of the tube bank, three planes are used. The positions are 43mm from the bottom for Plane 1 (P1), 73mm from the bottom for Plane 2 (P2) and 103mm from the bottom for Plane 3 (P3), as can be observed in Figure 2 b). The force coefficients are obtained with the integrated pressure on the area, data from the cylinder diameter and gap velocity.

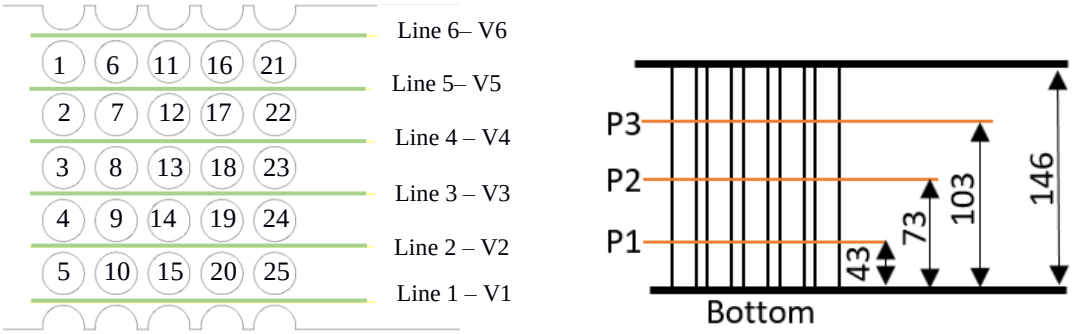

(a) (b)

Figure 2. a) Positions of monitoring velocity and b) planes along the domain height.

3. RESULTS

The results from the Large Eddy Simulation, presented for pressure and velocity planes, show the flow around the bank of fixed tubes. In Figure 3 a) and d) the plane is 0.043m from the bottom, the plane in Figure 3 b) and e) is 0.073m from the bottom and in Figure 3 c) the plane is 0.103m from the bottom, as shown in Figure 2 b).

In Figure 3 a) the asymmetric flow around the cylinders is observed after the second row, the flow decreases behind the cylinders 7 and 8. The gap between the cylinders shows a significant change of the velocity magnitude with an increase between the cylinders 13 and 14, decrease between 12 and 13. The wake asymmetry in the last row is visible, with a wide wake behind the cylinder 21. The pressure plane in Figure 3 d) also shows the pressure asymmetry around cylinders 7 and 8, but in the front cylinder showing higher pressure than the additional cylinders.

In Figure 3 b) the asymmetric flow is clear after the second row of cylinders, where after cylinder 7 and cylinder 8, the flow deviates from the main downward path. At this point, the deviation involves most cylinders after the second row. The pressure results in Figure 3 e) show pressure increase in front of the cylinder, mainly for second row. The asymmetric flow in the last row show wide wake behind cylinder 21 and 23.

In Figure 3 c) the asymmetry of the flow is clear after the cylinder 16 and, in this case, the upward deflection. This redistribution can be seen in the magnitude of the velocity within the tube bank and, to quantify these changes, the velocity is plotted on the lines shown in Figure 2 a), for the central plane. The velocity in Figure 4 is non-dimensional, where the input velocity was used.

The wakes after the bank of tubes present alter the characteristic of along the height. In Figure 3 a) and c) the wake is narrow behind the cylinder 23, but in Figure 3 b) the wake is wide. Changing the wake mode indicates the redistribution of the flow over the height between the rows of cylinders, where disturbances within the tube bank can alternate the flow from that region forward. The drop pressure has different magnitudes along the height of the tube bank in Figure 3 d) and e) the pressure is lower between the third and fourth line than the pressure in Figure 3 f).

In Figure 4, the velocity along the gap, as shown in Figure 2 a), is plotted, it is observed that until the first line the flow is uniform, after the first line begins to increase or decrease the velocity between the lines. After the second row, the differences between rows increase on Line 1 and Line 3 show a velocity decrease. In the additional rows, the difference increases and decreases according to the analyzed position.

The results presented in Figure 3 and Figure 4 show the characteristics described by Olinto et al. (2009) who, with the visualization of the flow using dye, observed the redirection of the flow within the tube bank. Iacovides et al. (2014) also reported asymmetry, but in this case, the authors linked the asymmetric change to the turbulent model adopted, but it could represent a physical response.

This mass redistribution may be the fluid instability that justifies some studies to present a significant cylinder vibration increase, Price and Paidöussis (1989), and others do not observe significant increase, Austermann and Popp (1994). Price and Paidöussis (1989), who carried out experiments in five rows, six columns with 1.5 p/d and the results for a single flexible tube located in the first five rows of the array on air showed instability at values higher than typical flow velocity for a fully flexible array. Another study by Austermann and Popp (1994) showed that stability limits of the flexibly mounted cylinder positioned in each of the first three or four rows of an in-line configuration did not show an

increase in the vibration amplitude. These stability thresholds for the free tube equilibrium position depend on the pattern of the array as well as the distance from the tube.

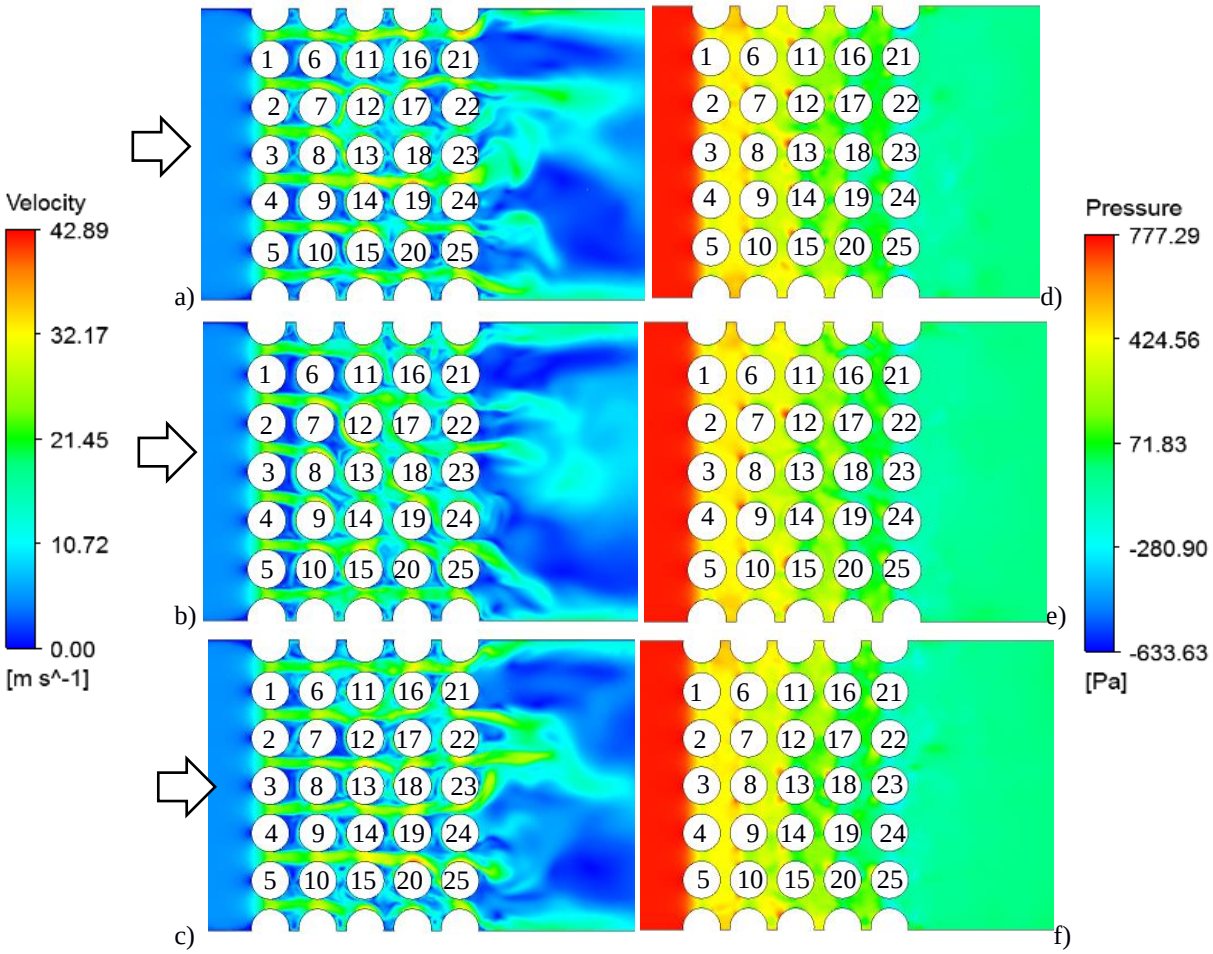

Figure 3. Velocity planes of the tube bank in a) 0.043m, b) 0.073m, c) 0.103m and Pressure planes of the tube bank in d) 0.043m, e) 0.073m, f) 0.103m.

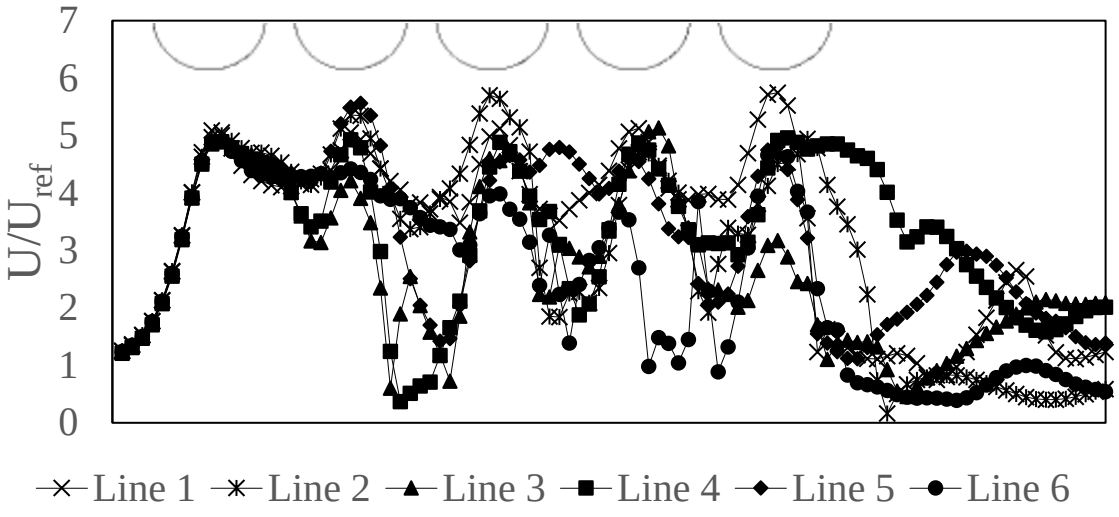

Figure 4. Non-dimensional velocity inside the gap for the height of 0.073m.

The force coefficient for each cylinder is obtained integrating the force, applying the non-dimension analysis based on the gap velocity in the first row. The drag force change along the tube bank can be seen in Table 1. The first row presents the highest values, as expected, due to the uniform inlet flow. Second row, from t6 to t10, the drag coefficient decreases with half the magnitudes obtained for the first row. The tubes at the extremity, t6 and t10, show the lower drag forces. In the third row, the central tube has the highest magnitude and the entire cylinder present increases the magnitude of the force comparing to the second row. In the fourth row, the magnitudes remain similar. The fifth row presents lowest values associated with t21 and t24.

The mean lift coefficient is presented in Table 2. In the first and second row, all cylinders have low magnitudes; in third row, two cylinders, t12 and t15, have significant magnitudes for lift and both tubes are related to the asymmetric flow in part of the cylinder height, as can be seen in Figure 3 a) and b). In the fourth row, the cylinders t18 and t20 show greater magnitude in the lifting force and an increase in velocity around t20 is visible in Figure 3c). In the fifth row, the cylinder t25 has a higher value.

Comparing the present results with da Silva et al. (2019) for p/d =1.5 and l/d = 2, the trend is similar with high values in the first row and reduction in the additional rows, but the magnitudes of drag coefficient are lower in the first row for the present study. The lift coefficients show results similar to the present case, the increase in lift forces is observed in some cylinders over time, but the authors represent the fluctuations and do not comment on the variation.

Table 1. Mean Drag coefficient in each cylinder.

Cyl.	C_d	Cyl.	C_d	Cyl.	C_d	Cyl.	C_d	Cyl.	C_d
t1	0.45	t6	0.22	t11	0.29	t16	0.32	t21	0.26
t2	0.47	t7	0.26	t12	0.32	t17	0.28	t22	0.34
t3	0.47	t8	0.25	t13	0.41	t18	0.30	t23	0.31
t4	0.48	t9	0.26	t14	0.36	t19	0.31	t24	0.21
t5	0.48	t10	0.20	t15	0.29	t20	0.33	t25	0.34

Table 2. Mean Lift coefficient in each cylinder.

Cyl.	C_L	Cyl.	C_L	Cyl.	C_L	Cyl.	C_L	Cyl.	C_L
t1	-0.03	t6	-0.06	t11	-0.04	t16	-0.06	t21	0.001
t2	0.01	t7	0.03	t12	-0.12	t17	-0.03	t22	0.06
t3	-0.03	t8	0.05	t13	-0.05	t18	-0.13	t23	-0,04
t4	-0.03	t9	-0.07	t14	0.04	t19	0.05	t24	-0.03
t5	0.02	t10	0.06	t15	0.14	t20	0.16	t25	0.10

The mean drag and lift coefficients are useful information for the global behavior, although the dynamic responses of a vibration process are related to instantaneous instabilities. Figure 5 shows the force in the direction X, instantaneous drag force, distribution for the first row, third and fifth rows. The force distribution in Figure 5 a) is uniform between the cylinders, in Figure 5 b) and c) there are regions of concentration of force with significant changes along the height. This behavior is also observed for the instantaneous lift force. Y direction distribution, shown in Figure 6. In the first row, Fig. 6 a), the distribution is uniform. In the third and fifth rows, Fig. 6 b) and c), regions with high or low forces are observed along the height.

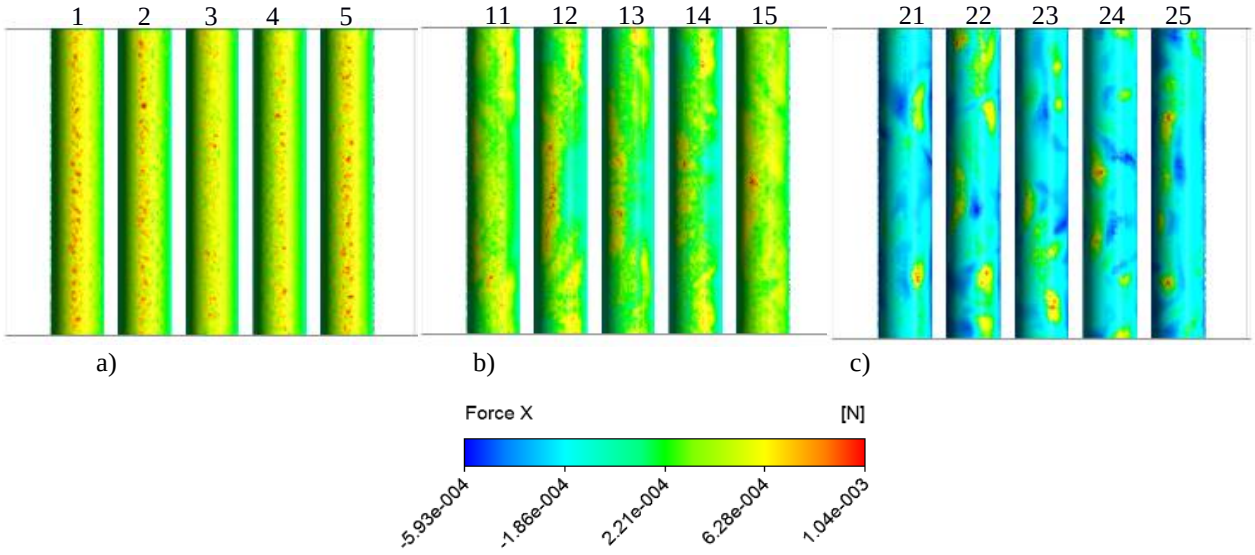

Figure 5. Drag force distribution in frontal view of the cylinder a) First Row, b) Third Row and c) Fifth Row.

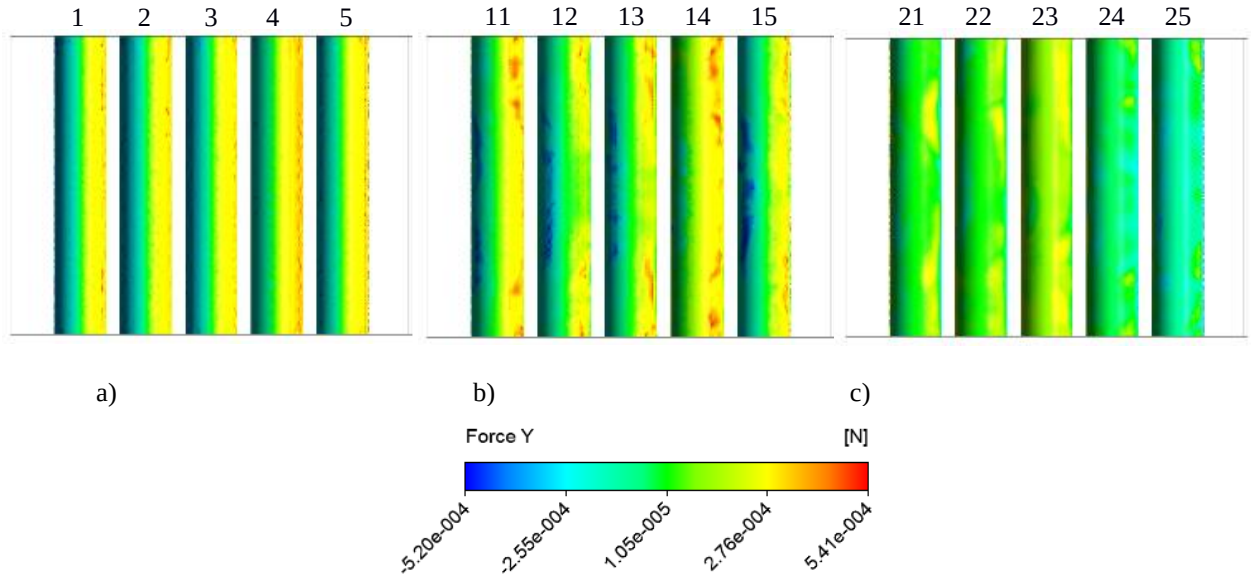

Figure 6. Force Y in frontal view of the cylinder a) First Row, b) Third Row and c) Fifth Row.

4. CONCLUSIONS

The study presented a numerical analysis for fixed tube banks with a square pitch ratio of P / D = 1.26 to investigate the asymmetric flow within the tube bank. Velocity, pressure and force are used to analyze the asymmetric flow.

The velocity and pressure contours at different heights in the tube bank showed an asymmetric distribution of both variables. The first-row velocity increase is due to the reduction in area, but in the additional lines is linked to a mass redistribution, as described by Olinto et al. (2009). The average forces present high drag coefficients in the first row and a reduction for additional rows. The lift coefficient has higher values in some tubes in each row.

The forces response can be linked to the velocity distribution inside the tube bank, where the magnitude of the velocity in each gap of the tube bank shows significant differences in the velocity magnitudes. The asymmetry observed on the velocity and pressure of the flow is the reason for the velocity and forces changes. The vibration response can be linked to the instantaneous force that can be responsible for an imbalance of the body and, related to the assembly characteristics such as damping and freedom of vibration, the cylinder can be unstable by exciting close to a natural frequency and increasing the amplitude of the vibration.

5. REFERENCES

ANSYS Fluent. 2018. Theory Guide.

Abed, N. and Afgan I. 2017. "A CFD study of flow quantities and heat transfer by changing a vertical to diameter ratio and horizontal to diameter ratio in inline tube banks using URANS turbulence models" *International Communications in Heat and Mass Transfer*, Vol. 89, p. 18–30.

Austermann, R. and Popp, K. 1995. "Stability behaviour of a single flexible cylinder in rigid tube arrays of different geometry subjected to cross-flow". *Journal of Fluids and Structures*, Vol. 9, p. 303-322.

Blevins, R. D. 1990. *Flow-Induced Vibration*. Second Edition. New York: Van Nostrand Reinhold.

Endres. L. A. M and Möller, S. V. 2009. "Experimental study of the propagation of a far-field disturbance in the turbulent flow through square array tube banks". *Journal of the Brazilian Society of Mechanical Sciences and Engineering*, Vol. XXXI, p. 232-242.

Iacovides, H., Launder, B. and West, A. 2014. "A comparison and assessment of approaches for modelling flow over in-line tube banks" *International Journal of Heat and Fluid Flow*, Vol. 49, p. 69–79.

Lesieur, M., Métais. O., Comte, P. 2005. *Large-Eddy Simulations of Turbulence*. Cambridge University press.

Olinto, C. R., Indrusiak, M. L. S., Endres, L. A. M. and Möller, S. V. 2009. "Experimental study of the characteristics of the flow in the first rows of tube banks" *Nuclear Engineering and Design*, Vol. 239, p. 2022–2034.

Päidoussis, M. P., Price, S. J., de Langre, E., 2011, *Fluid-Structure Interactions: Cross-Flow-Induced Instabilities*. Cambridge University Press, New York.

Price, S. J. and Païdoussis, M. P. 1989. "The flow-induced response of a single flexible cylinder in an in-line array of rigid cylinders". *Journal of Fluids and Structures*, Vol. 3, p. 61-82.

Da Silva, B. L., Luciano, R. D., Utzig, J. and Meier H. F. 2019. "Analysis of flow behavior and fluid forces in large cylinder bundles by numerical simulations". *International Journal of Heat and Fluid Flow*, Vol. 75, p. 209–226,

Wilcox, D. C. 1993. *Turbulence Modelling for CFD*. First Edition. California. DCW Industries.

6. RESPONSIBILITY NOTICE

The authors are the only responsible for the printed material included in this paper.